Example 2, continued.

To demonstrate the utility of this methodology, we applied it to a complex geometry in a coastal domain off Massachusetts. Velocity and diffusivity fields were specified from a simulation of the March-April climatological flow (Figure 1). [An alternative representation of the hydrodynamic field in terms of streamfunction is shown in Figure 2; we need to choose one of these two figures.] The basis of these simulations is a fully nonlinear, three-dimensional primitive equation model with turbulence closure (Lynch *et al.*, 1996). This model has been used extensively to study coastal currents in this region, particularly in the area north of Cape Cod (Lynch *et al.*, 1997). Archived solutions (see `http://www-nml.dartmouth.edu/CircMods/`) were vertically averaged to obtain D and $\mathbf{V}$ fields suitable for use in Equation (21). The circulation is dominated by a southward flowing coastal current, which partially bifurcates south of Cape Ann. During this time period, a small portion of the current splits off and flows through Massachusetts and Cape Cod Bays. This branch subsequently rejoins the bulk of the coastal current off the northern tip of Cape Cod, where the southward flow intensifies (note that the fine mesh on the steep topography east of Cape Cod makes the current appear more intensified in Figure 1 than it actually is). The highest diffusivities (in excess of 500 m^2s^{-1} are associated with Martha's Vineyard and Nantucket islands south of Cape Cod; another local maximum (on the order of 400 m^2s^{-1} is located west-northwest of the northern tip of Cape Cod. Elsewhere, diffusivity is on the order of 100 m^2s^{-1}. Flow in the deeper areas offshore is generally sluggish compared to the coastal current.

Covariance structures C_{uu} for various nodes off the Cape Cod shoreline illustrate the impact of the coastal geometry and transport fields (Figure 3). Information on nodes along the northeast coast of Cape Cod (upper two panels) spreads southward with the coastal current. In addition, there is significant propagation of information in the "upstream" direction owing to the very high diffusivity present along the northern tip of Cape Cod, with significant covariance penetrating all the way into Cape Cod Bay. In contrast, the covariance structure associated with a node in the southeast corner of Cape Cod Bay is confined to the bay itself, due to the weak currents and low diffusivity present in that region. Similarly, covariance with a node off the southern shore of Cape Cod is limited to Vineyard and Nantucket Sounds. These latter two examples highlight the fact that the coastal geometry is built in to the covariance structure, as information clearly does not propagate across land boundaries.

An example objective analysis is shown in Figure 4a. The data are observed concentrations of the toxic dinoflagellate *Alexandrium* spp. from a survey conducted in 1993 as part of the Regional Marine Research Program in the Gulf of Maine. Control parameters for the objective analysis (Table 1) were chosen as follows. The observational noise n was set to the precision of the measurement, which is 10 cells l^{-1}. The first-order decay constant k^2 in Equation (21) sets the horizontal scale of patchiness in the absence of advection and process noise. For a purely diffusive balance ($D\nabla^2 u \sim k^2 u$), the non-dimensional ratio $\frac{\sqrt{D}}{k}$ is the e-folding scale for patches of u. Assuming a typical patch size of 1 km and a diffusivity of 100 m^2 s^{-1} yields $k^2 = 1.0 \cdot 10^{-4}$. The process noise is scaled to meet the variance of the observations in the absence of hydrodynamic transport in Equation (21):

$$Var(\epsilon) \sim Var(k^2 u)$$

This particular data set has a mean of 92 cells l^{-1} and a standard deviation of 142 cells l^{-1}, resulting in an estimated process noise of $\epsilon = 1.42 \cdot 10^{-2}$ cells l^{-1} s^{-1}. The spatial scale of the process noise is assumed to be 2 km.

Although the observed distribution is quite patchy, abundance is generally high in Massachusetts Bay and low elsewhere (Figure 4a). The objectively analyzed field captures the essence of this pattern, spreading information according to the covariance structure determined by the hydrodynamics and assumptions about the underlying process. Note that the analyzed field does not match the observations exactly; smoothing is implied by the first-order decay specified in Equation (21), and there is noise associated with both the observations and the process. The accompanying map of standard error (Figure 4b) is simply the square root of the diagonal of $C_{\tilde{u}\tilde{u}}$. Expected error is reduced in the vicinity of the observations, and generally rises to the standard deviation of the data elsewhere. Note that there is structure in the standard error in the far field, where the posterior covariance $C_{\tilde{u}\tilde{u}}$ is no different from the prior covariance C_{uu}. This structure comes as a direct result of the hydrodynamic field. For example, the very high diffusivity near Martha's Vineyard and Nantucket island would tend to smooth any patchiness in that area, thereby reducing the expected variance.

Comparison of these objectively analyzed distributions with maps of the same data made with straightforward interpolation techniques demonstrates the utility of this approach. For example, cubic spline interpolation can be used to fill the gaps in between data points (Figure 5). With such an algorithm, the resolution of the mesh determines the spatial scale of the interpolated structures. The resulting fields are typically truncated beyond the areas of data coverage (Figure 5a). Various techniques can be used to force the extrapolation problem, such as the introduction of artificial data points in the far field (*e.g.*, Figure 5b). However, this *ad hoc* procedure has obvious shortcomings. The objective analysis technique described herein thus has clear advantages in that it accounts for coastal geometry, a specified hydrodynamic field, and an explicit mathematical representation of the underlying processes controlling the distribution of the quantity being mapped.

Acknowledgments

We are grateful to D. Anderson, B. Keafer and R. Signell for providing the *Alexandrium* spp. data used in Figures XX and XX+1. Those data were collected as part of the Regional Marine Research Program for the Gulf of Maine, Project GMR-20. Additional support for this research was provided by NOAA and NSF through the ECOHAB-GOM and Globec programs.

Parameter	Value	Definition
n	10 cells l^{-1}	observational noise
k^2	$1.0 \cdot 10^{-4}$ s^{-1}	first-order decay coefficient
ϵ	$1.42 \cdot 10^{-2}$ cells l^{-1} s^{-1}	process noise
r	2 km	spatial scale of process noise

Table 1: Objective analysis control parameters for Example 2.

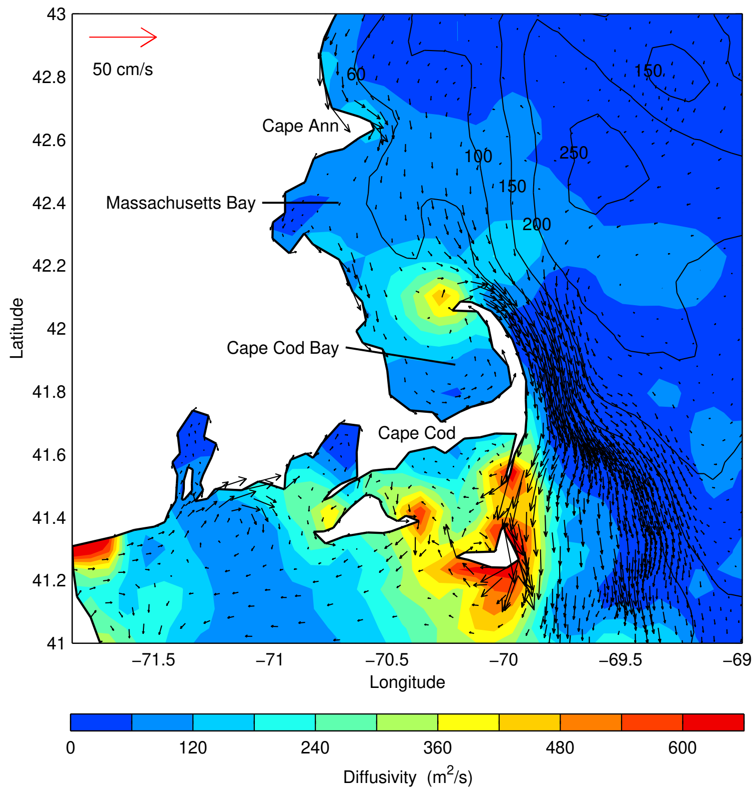

Figure 1: Climatological velocity and diffusivity fields for the March-April time period. The scale for the velocity vectors appears in the upper left. Selected bathymetric contours are overlayed.

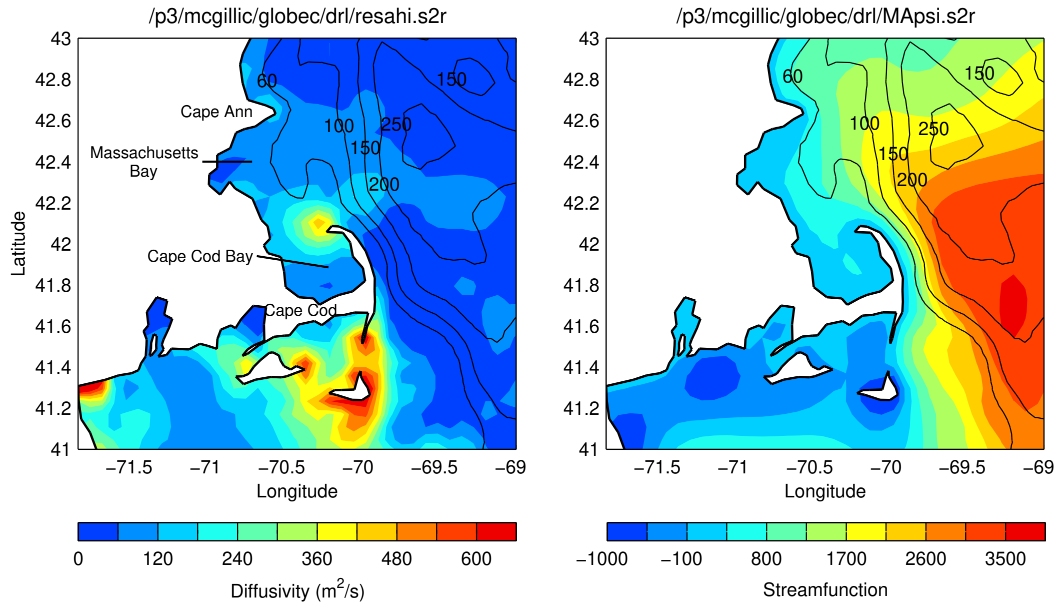

Figure 2: Climatological diffusivity and streamfunction fields for the March-April time period. Selected bathymetric contours are overlayed.

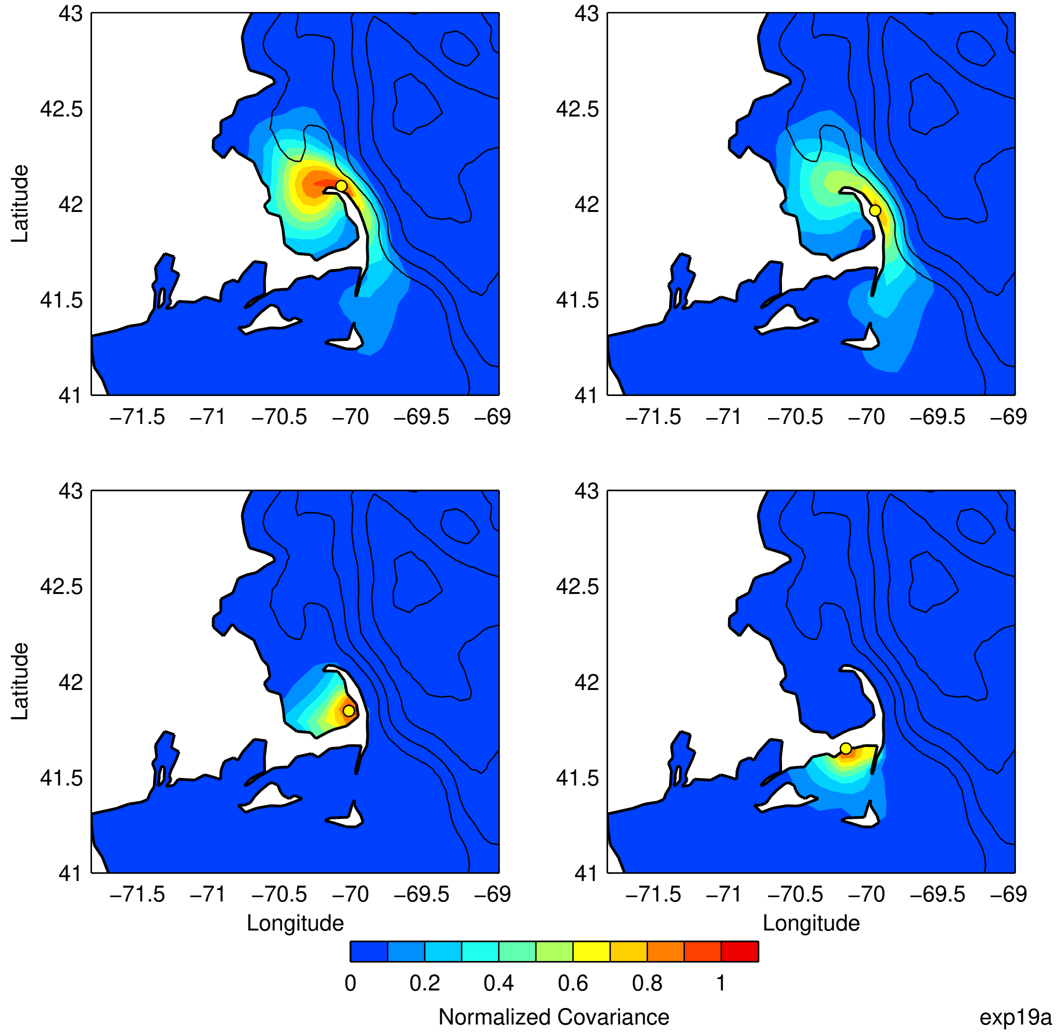

Figure 3: Normalized covariance structures of four nodes off the Cape Cod shoreline. In each case the covariance is normalized to the value at the node in question (indicated by a white dot). In this example, $k^2 = 2.0 \cdot 10^{-6}$ and $\epsilon = 2.0 \cdot 10^{-6}$. The spatial scale of the process noise is specified to be $2.0 \cdot 10^3$m.

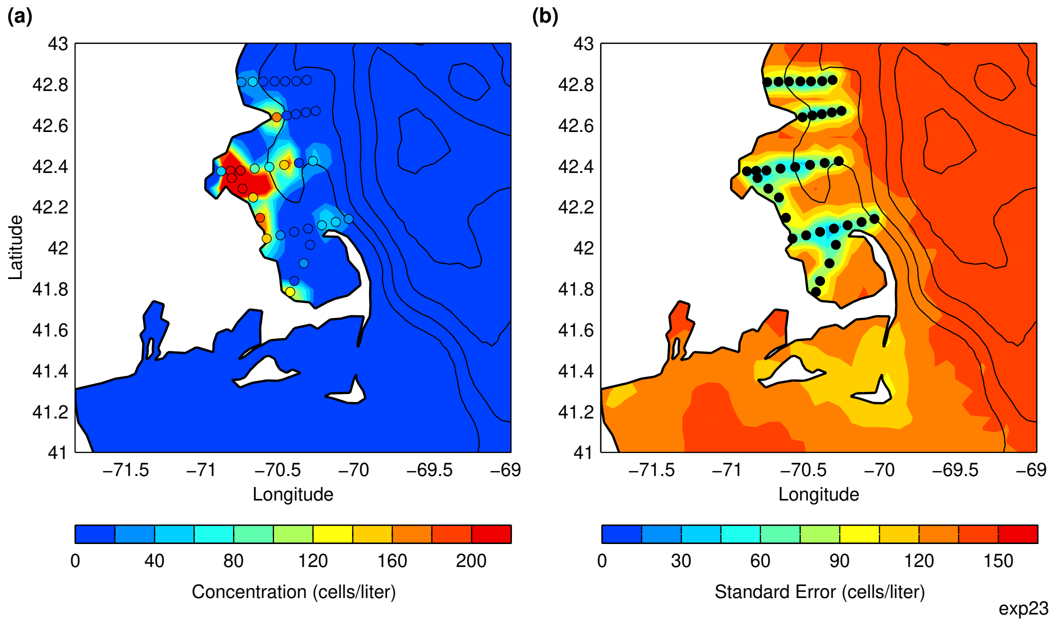

Figure 4: (A) Objective analysis of *Alexandrium* spp. concentration. Observed values are shown as colored dots, with the same color scale used to map the objectively analyzed field. (B) Standard error estimate, $C_{\tilde{u}\tilde{u}}^{\frac{1}{2}}$.

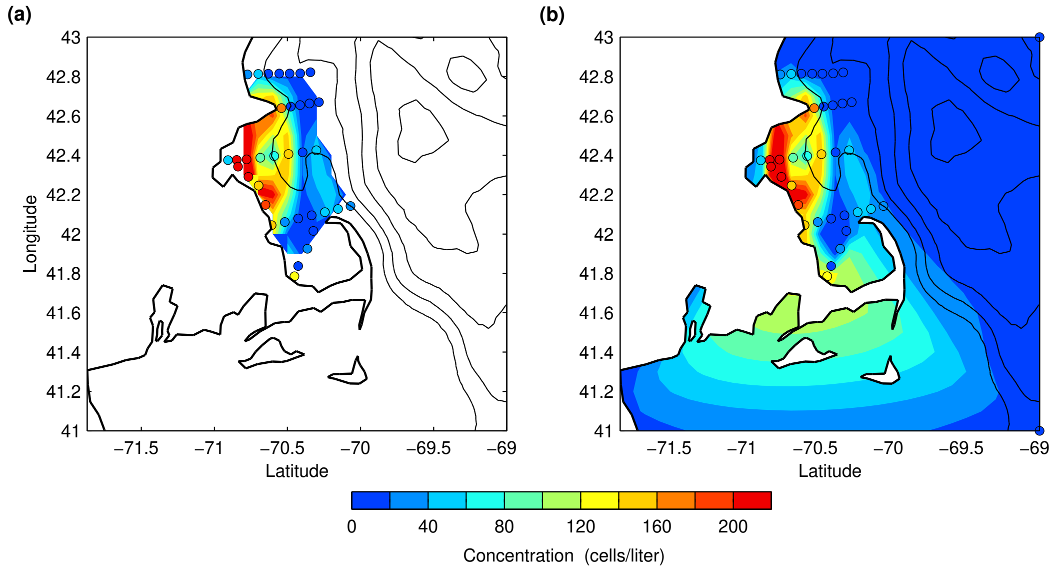

Figure 5: (A) Cubic interpolation of the same *Alexandrium* spp. concentration data shown in Figure 4a. Observed values are shown as colored dots. The field is truncated in areas where extrapolation is required. (B) Remapping of (A) in which artificial data points (of zero concentration) are inserted at the corners of the mapping domain in order to force the interpolator to fill the entire field.